Faraday Discussions

Accepted Manuscript

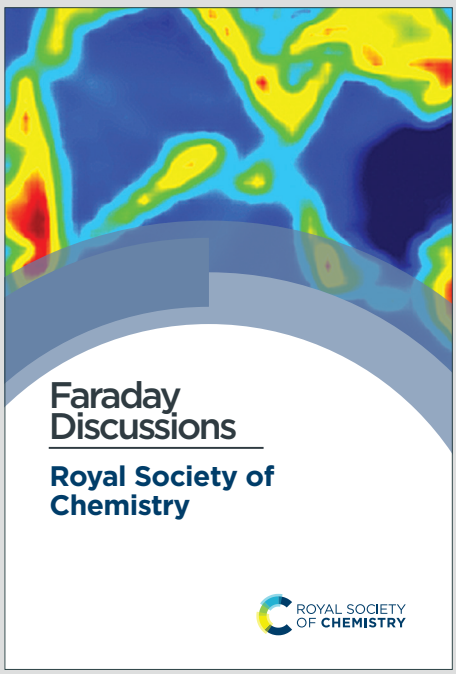

This article can be cited before page numbers have been issued, to do this please use: J. Park, S. Park, S. Park, H. Cho, D. C. Lee and B. Shin, *Faraday Discuss.*, 2026, DOI: 10.1039/D6FD00036C.

ROYAL SOCIETY OF CHEMISTRY

www.rsc.org/faraday_d

Faraday Discussions

View Article Online
DOI: 10.1039/D6FD00036C

PAPER

Phase Regulation via Dual Additives for Pure-blue Emitting Quasi-2D Perovskite Light Emitting Diodes

Jinu Park,*[a] Seoyeon Park,*[a] Seongju Park,[a] Hyunjin Cho,[b] Doh C. Lee[b] and Byungha Shin†[a]

a) Department of Materials Science and Engineering, Korea Advanced Institute of Science and Technology (KAIST), Dae-jeon 34141, Republic of Korea

b) Department of Chemical and Biomolecular Engineering, Korea Advanced Institute of Science and Technology (KAIST), Dae-jeon 34141, Republic of Korea

†Corresponding authors: byungha@kaist.ac.kr

Received 00th January 20xx, Accepted 00th January 20xx
DOI: 10.1039/x0xx00000x

Abstract

Solution-processed mixed-halide quasi-2-dimensional (quasi-2D) perovskites offer precise bandgap tunability and high color purity, and their moderate exciton binding energies enable efficient inter-phase energy funneling, from wide-bandgap lower-*n* (where *n* denotes the number of inorganic octahedral layers in the quasi-2D lattice) phases to narrower-bandgap larger-*n* phases, that concentrates excitations in the emissive phase and supports high emission efficiencies. Achieving pure-blue emission, however, often requires heavy spacer loading (e.g., phenethylammonium, PEA^+), which overproduces low-*n* ($n \leq 3$) domains with excessively high exciton binding energies, thereby intensifying Auger recombination and diminishing inter-phase funneling. Compounding these effects, ion migration/halide redistribution, halide-vacancy-induced under-coordinated Pb^{2+} centers, and charge-injection imbalance collectively undermine the stability of blue devices. This study exploits the synergy of bis(triphenylphosphine)iminium chloride (PPNCl) and cesium trifluoroacetate (CsTFA) to tune spacer–perovskite binding while passivating Pb^{2+} centers and halide vacancies. Cl^- widens the bandgap of large-*n* phases, enabling pure-blue emission, and the $[PPN]^+$ cation acts as an electron donor that forms hydrogen bonds with PEA^+, thereby strengthening spacer–perovskite interactions. This interaction reconstructs the quasi-2D *n* phase distribution. Similarly, TFA^-, enabled by the high electronegativity of its F substituents, forms hydrogen bonds with PEA^+ and promotes *n* phase redistribution. Together, these effects markedly deplete low-dimensional phases ($n = 2, 3$), the primary contributors to non-radiative recombination, and suppress the emergence of bulk 3D phases with low exciton binding energy. They also enhance inter-phase energy transfer, as confirmed by transient absorption spectroscopy (TAS). Additionally, the additives effectively passivate halide vacancies and suppress metallic Pb formation, further improving device performance. Compared with devices relying solely on $PbBr_2/PbCl_2$ ratio tuning, this approach delivers superior spectral stability. The resulting devices achieve pure-blue emission at 473 nm, with external quantum efficiency (EQE) = 8%, peak luminance = 350 cd/m^2, and a narrow full width at half maximum (FWHM) of 21 nm; notably, electroluminescence peak shifts are limited to ≤ 3 nm during operation, ensuring excellent spectral stability. These results represent a significant advancement in quasi-2D mixed-halide perovskite LEDs, offering a promising pathway for the development of stable and efficient pure-blue perovskite light-emitting diodes.

Introduction

Metal halide perovskites (MHPs) have emerged as promising light emitters for next-generation displays, owing to their high color purity, high photoluminescence quantum yield (PLQY), and compatibility with low-cost solution processing.[1–4] Perovskite light-emitting diodes (PeLEDs) in the green, red, and near-infrared regions have already surpassed 25% external quantum efficiency (EQE).[5–8] In contrast, achieving comparable performance in the blue and deep-blue regimes remains challenging. In particular, the development of efficient and operationally stable pure-blue PeLEDs that satisfy the stringent Rec. 2020 window (460-475 nm) is a key bottleneck for realizing full-color perovskite-based displays.[2,10,11]

Conventional strategies to achieve pure-blue emission confront fundamental challenges. Compositional engineering via halide mixing (Br/Cl) in three-dimensional (3D) perovskites effectively widens the bandgap, yet the intrinsically low exciton binding energy (E_b) limits radiative efficiency,[12] and electric-field-induced halide segregation compromises spectral stability.[4,9,13] Alternatively, dimensional engineering to form low-dimensional bromide-only perovskites leverages quantum confinement to reach the blue regime. However, restricting the framework to highly confined low-dimensional phases (e.g., $n \leq 3$, where n is the number of octahedral layers) necessitates an excessive fraction of insulating organic spacers. This inherently compromises charge-carrier mobility and introduces a high density of non-radiative surface defects, severely limiting device efficiency.[1,14–16] Furthermore, extreme quantum confinement significantly accelerates Auger recombination, a major non-radiative loss pathway, leading to severe efficiency roll-off under device operation.[17–19]

Rational convergence of these two strategies provides a pathway to bypass these limitations; incorporating Cl to reach the pure-blue bandgap while utilizing a minimal number of bulky spacers to fundamentally inhibit pure 3D phase formation and maintain sufficient E_b. Yet, this hybrid approach introduces its own set of challenges. First, even when precursor stoichiometry is designed to target a specific n value, similar formation energies among $n \geq 3$ phases and the preferential consumption of spacers during early formation of low-n phases often lead to the unintended emergence of large-n phases.[20] Consequently, the film typically contains a distribution of n phases rather than a single targeted phase; this spontaneous phase heterogeneity drives uncontrolled energy funneling and shifts the emission away from the target pure-blue color.[21] Second, the incorporation of chloride is often hindered by the poor solubility of conventional chloride precursors (e.g., $PbCl_2$, CsCl) in standard processing solvents.[9] Furthermore, these mixed-halide phases suffer from intrinsic thermodynamic instability; under operational electric fields, they readily undergo ion-migration-driven phase segregation, leading to severe spectral drift during device operation.[22,23]

Herein, we demonstrate a synergistic dual-additive strategy that simultaneously resolves the phase-heterogeneity and spectral-instability bottlenecks in quasi-two-dimensional (quasi-2D) mixed-halide perovskites. We employ bis(triphenylphosphine)iminium chloride (PPNCl) not merely as an additional chloride source, but as a multifunctional structural and electronic regulator. Its resonance-stabilized phosphazene framework, featuring a conjugated Ph–P=N=P motif, enriches electron density at the nitrogen site.[4] This electronic structure enables strong coordination with Pb^{2+} and promotes hydrogen bonding with the spacer cation. These dual interactions not only steer phase formation by regulating spacer-perovskite binding but also facilitate chloride incorporation into the lattice, thereby suppressing halide-vacancy formation and mitigating phase segregation.[16] The highly electronegative fluorinated carboxylate group of CsTFA synergizes with PPNCl to sterically immobilize bulky spacers and passivate residual halide vacancies. Through this cooperative binding dynamics, the phase distribution is focused on highly emissive, defect-suppressed large-n phase ($n \geq 5$), effectively dismantling the non-radiative recombination pathways typical of low-n phases while arresting halide segregation.[24]

Consequently, our dual-additive approach yields pure-blue quasi-2D mixed-halide emitters with a narrow photoluminescence peak at 467 nm. The resulting PeLEDs exhibit spectrally stable pure-blue electroluminescence (EL) at 473 nm, with negligible spectral drift ($\leq$ 3 nm), a maximum EQE of 8.0%, and a maximum luminance of 350 cd/m^2. Beyond the immediate performance metrics, this work establishes a versatile molecular engineering paradigm to decouple the fundamental trade-offs between charge transport, quantum confinement, and color stability in blue perovskite emitters.

Methods

Materials

All chemicals were used as received without further purification. Cesium bromide (CsBr, 99.999%), lead bromide ($PbBr_2$, 99.999%), lead chloride ($PbCl_2$, 99.999%), guanidinium bromide (GABr, ≥98%), lithium bromide (LiBr, 99.995%), bis(triphenylphosphoranylidene)ammonium chloride (PPNCl, 97%), dimethyl sulfoxide (DMSO, 99.9%), ethyl acetate (EA, 99.9%), acetone, and isopropyl alcohol (IPA) were purchased from Sigma-Aldrich and DUCKSAN. Phenethylammonium bromide (PEABr) and formamidinium bromide (FABr, 99.99%) were obtained from Greatcell Solar Materials, and cesium trifluoroacetate (CsTFA, 98%) was sourced from Thermo Scientific Chemicals. Polymeric and interfacial materials, including poly(3,4-ethylenedioxythiophene):poly(styrenesulfonate) (PEDOT:PSS, Clevios™ P VP Al 4083, Heraeus) and 4,4′,4″-tris(carbazol-9-yl)triphenylamine (TCTA, Lumtec), were used as received. 1,3,5-tris(1-phenyl-1H-benzimidazol-2-yl)benzene (TPBi, Lumtec), lithium fluoride (LiF), and aluminum (Al) were obtained from commercial suppliers.

Preparation of quasi-2D perovskite precursor solutions

View Article Online
DOI: 10.1039/D6FD00036C

PEABr, CsBr, $PbBr_2$, $PbCl_2$, FABr, GABr, and LiBr were dissolved in DMSO at room temperature and stirred overnight to afford clear precursor solutions. The molar ratio of PEABr:CsBr:$PbBr_2$:$PbCl_2$:FABr:GABr:LiBr was fixed at 0.8:1:0.8:1.2:0.1:0.1:0.1, and the total concentration was adjusted to 0.1 M with respect to the total Pb content. For additive incorporation, bis(triphenylphosphoranylidene)ammonium chloride (PPNCl) and cesium trifluoroacetate (CsTFA) were introduced at 5 mol% and 10 mol%, respectively, relative to the total Pb molar amount.

Device Fabrication

ITO-coated glass substrates (ITO thickness: 150 nm) were sequentially sonicated for 15 min each in deionized water, acetone, and isopropyl alcohol, and then treated with UV–ozone for 20 min. PEDOT:PSS was spin-coated onto the cleaned ITO substrates at 4000 rpm for 40 s and annealed at 150 °C for 20 min. A TCTA interlayer (4 mg/mL in toluene) was subsequently spin-coated at 4000 rpm for 30 s and annealed at 120 °C for 15 min. The perovskite layer was deposited by spin-coating 80 μL of the precursor solution onto the TCTA layer at 5000 rpm for 60 s. Ethyl acetate (200 μL) was dynamically dispensed as an antisolvent 30 s after the start of spinning. The resulting films were annealed at 80 °C for 5 min. Electron-transport and electrode layers were then deposited by thermal evaporation under high vacuum: TPBi (50 nm), LiF (2 nm), and Al (100 nm). The device active area, defined by the overlap between the ITO and patterned Al electrodes, was 5 mm^2.

Characterization

X-ray Diffraction (XRD): XRD patterns of the perovskite films were collected using a SmartLab diffractometer (RIGAKU) with Cu Kα radiation (λ = 0.154 nm) at the KAIST Analysis Center for Research Advancement (KARA).

Grazing Incidence X-ray Diffraction (GIXRD): GIXRD measurements of the quasi-2D perovskite films were performed on a SmartLab system (RIGAKU) equipped with a micro-focus Cu rotating anode (1.2 kW) and Cu Kα radiation (λ = 0.154 nm). Data were acquired at an incidence angle of 0.3° at KARA.

X-ray Photoelectron Spectroscopy (XPS): XPS spectra were obtained at KARA using a Sigma Probe system (Thermo VG Scientific) with a He I ultraviolet source (21.22 eV).

Steady-state PL and Absorption: Steady-state PL spectra were recorded on an F-7000 FL spectrophotometer (HITACHI) with an excitation wavelength of 370 nm. UV–Vis absorption spectra were measured using a UV-1800 spectrophotometer (SHIMADZU).

Photoluminescence Quantum Yield (PLQY): PLQY was measured with a C13534-11 Quantaurus-QY Plus UV–NIR spectrometer (HAMAMATSU).

Time-Resolved PL (TRPL): TRPL decays and temperature-dependent PL measurements were conducted at KARA using a Fluorolog-QM spectrometer equipped with time-correlated single-photon counting (TCSPC) (HORIBA SCIENTIFIC), employing 375 nm excitation.

Transient Absorption Spectroscopy (TA): TA experiments were carried out using a regeneratively amplified Yb:KGW laser (Pharos, Light Conversion; 1028 nm, 196 fs, 200 kHz). A 360 nm pump beam was generated as the second harmonic of an optical parametric amplifier (Orpheus, Light Conversion). The probe was produced via white-light continuum generation in a sapphire plate. The probe beam (radius ~105 μm) was focused onto the sample and spatially overlapped with the pump. Signals were collected using a TA spectrometer (Harpia, Light Conversion) coupled with a Kymera 193i spectrograph (Andor).

J–V–L Characteristics and EL Spectra: Current density–voltage–luminance (J–V–L) characteristics and electroluminescence (EL) spectra were measured using a Keithley 2635A source meter and a CS-2000 spectroradiometer.

Nuclear Magnetic Resonance (NMR): ^{1}H, ^{19}F, and ^{31}P NMR spectra of PEABr, PPNCl, and CsTFA were acquired on an Avance Neo 600 spectrometer (Bruker) at KARA. Samples were prepared in DMSO-d6 (99.9 atom% D, Sigma-Aldrich) before measurement.

Results and Discussion

EL Characterization of Additive-Driven Improvements in Pure-Blue Emission

Blue perovskite LEDs were fabricated with the architecture Glass/ITO/PEDOT:PSS/perovskite/TPBi/LiF/Al (**Figure 1a**). In the additive-free reference device, the initial EL peak was located at 472 nm, but the spectrum was highly unstable: across the voltage range required to reach maximum luminance (up to ~8.5 V), the EL peak exhibited a pronounced shift of ~16 nm (**Figure 1b**). By contrast, devices incorporating PPNCl alone or together with CsTFA exhibited an initial EL peak at 472 nm and markedly suppressed spectral drift; within the operating range to maximum luminance (up to ~6 V), the EL peak shift was reduced to 4 nm for PPNCl and 2 nm for PPNCl + CsTFA (**Figure 1c, d**). Beyond

spectral stabilization, additive incorporation improved carrier injection over the full operating window, lowering the turn-on voltage (defined at 1 cd/m^2) from 4.6 V for the reference device to 3.6 V (**Figure 1e**). Notably, the PPNCl + CsTFA combination exhibited the lowest shunt-path current and the highest injection current above the operating threshold, consistent with more efficient charge injection and reduced leakage.

View Article Online
DOI: 10.1039/D6FD00036C

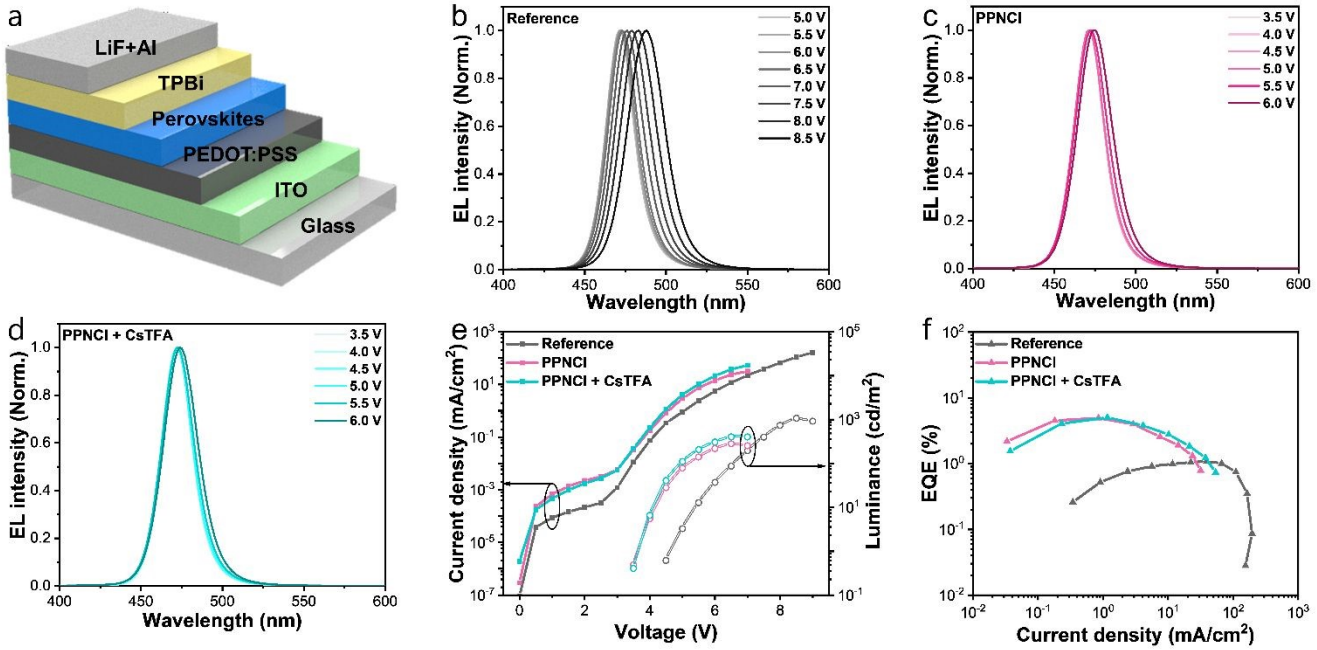

Figure 1. EL characteristics under various additive Conditions. (a) Perovskite LED structure. EL spectra under bias for (b) Br/Cl ratio-adjusted conditions, (c) PPNCl-introduced conditions, and (d) PPNCl + CsTFA-introduced conditions. (e) Current density-voltage-luminance (J-V-L) curves for conditions with pure blue emission tuned via simple $PbBr_2/PbCl_2$ ratio adjustment (black), PPNCl introduction (magenta), and PPNCl + CsTFA introduction (cyan). (f) Current density-external quantum efficiency (J-EQE) curves for each condition.

Accordingly, the maximum luminance increased to 280 cd/m^2 for PPNCl and to 405 cd/m^2 for PPNCl + CsTFA. In contrast, a meaningful maximum luminance for the reference device could not be defined because the large EL peak shift artificially inflates the apparent luminance under photopic weighting, and when evaluated at the same EL peak position, the luminance is only 13 cd/m^2. Consistent with these improvements, the maximum EQE increased from 1.08% in the reference device to 4.92% with PPNCl and 5.03% with PPNCl + CsTFA, corresponding to an approximately fivefold enhancement (**Figure 1f**).

Phase distribution engineering and exciton dynamics

To assess how the introduced additives modify the perovskite structure, the film structural characteristics were examined by absorption spectroscopy and grazing-incidence X-ray diffraction (GIXRD). In the absorption spectra, incorporation of PPNCl decreased the n = 2

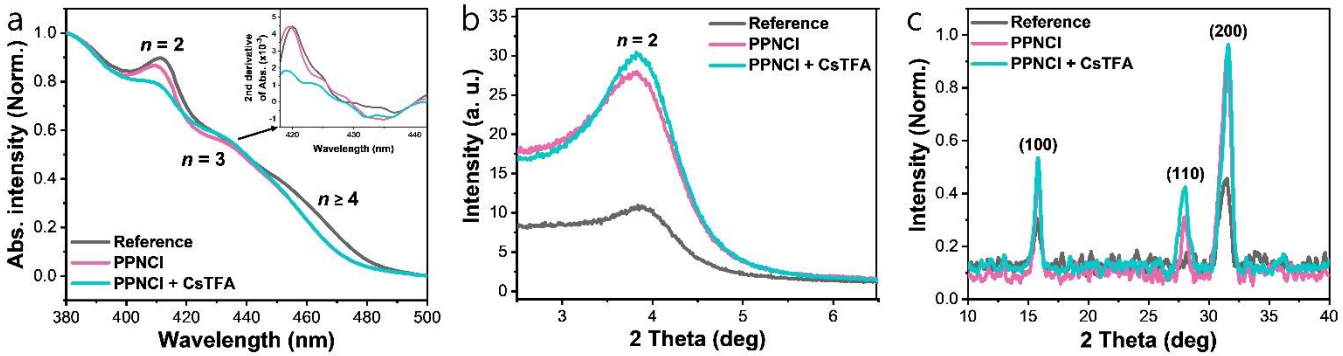

Figure 2. Structural impact of PPNCl and CsTFA on perovskite phases and crystallinity. (a) UV-vis absorption spectra of perovskite films under various additive conditions. The inset highlights the second derivative of the absorption spectra, corresponding to the n = 3 phase. (b) Grazing-incidence X-ray diffraction patterns of perovskite films under various additive conditions, focusing on the low-dimensional range. (c) X-ray diffraction patterns of perovskite films under various additive conditions.

population (absorption at 411 nm) and slightly increased the n = 3 contribution (absorption at 435 nm). It also widened the bandgap of the large-n ($n \geq 4$) phase, consistent with increased Cl^- content (**Figure 2a**). Upon further addition of CsTFA, the n = 2-related absorption feature was markedly suppressed, indicating an additional reduction of the n = 2 phase fraction. Despite the reduced fraction, GIXRD revealed improved alignment of the n = 2 phase (2θ = 3.8) in the low-dimensional region, suggesting a more oriented structure (**Figure 2b**), and the XRD patterns showed enhanced crystallinity along the {100} family planes (**Figure 2c**).

To further probe additive-induced changes in phase distribution and carrier funneling, transient absorption spectroscopy (TAS) was conducted (**Figure 3**). Ground-state bleaching (GSB) features were observed at wavelengths assigned to the n = 2, 3, 4, and ≥ 5 phases (413 nm, 435 nm, 452 nm, and 461 nm, respectively), consistent with steady-state absorption. In the bare film, pronounced GSB signals at n = 2 and n = 3 were accompanied by weak GSB intensity from the radiative large-n ($n \geq 5$) phase, implying a phase distribution biased toward low-n phases. Under this condition, the energy-funnelling process was inefficient, with exciton resonance persisting in the low-dimensional phases beyond 1000 ps. With PPNCl treatment, the GSB signals from low-n phases were substantially reduced, consistent with an increased large-n fraction, and the exciton resonance in the low-dimensional phases shortened to ~100 ps. When CsTFA was additionally incorporated, the resonance duration further decreased to ~10 ps. Moreover, the radiative large-n phase GSB linewidth was narrowest for the PPNCl + CsTFA condition, with an FWHM of 23 nm, suggesting effective defect passivation. Collectively, these TAS results indicate that the additives mitigate phase-distribution imbalance and enhance carrier-transfer efficiency.

To quantify the impact of phase-composition modulation on exciton dynamics, exciton rise and decay times were extracted for each n phase under each condition (**Figure 3g-i, Table S1**). PPNCl and CsTFA accelerated exciton decay, in the n = 2, n = 3, and n = 4 phases, with decay times decreasing from 0.53 to 0.13 ps, from 0.36 to 0.25 ps, and from 1.36 to 0.33 ps, respectively. In the radiative large-n phase, the exciton rise time decreased from 0.32 to 0.13 ps, indicating faster population build-up consistent with improved initial exciton generation and/or transport. Along with enhanced carrier-transfer efficiency, the large-n ($n \geq 5$) exciton decay time also decreased from 149 to 44 ps. The photoluminescence quantum yield (PLQY) and time-resolved photoluminescence (TRPL) results further support these trends. Additive incorporation increased the PLQY from 17% in the reference film to a maximum of 32%, and slightly narrowed the emission linewidth from 23 nm to 22 nm (**Figure S1, Table S2**). This linewidth reduction is

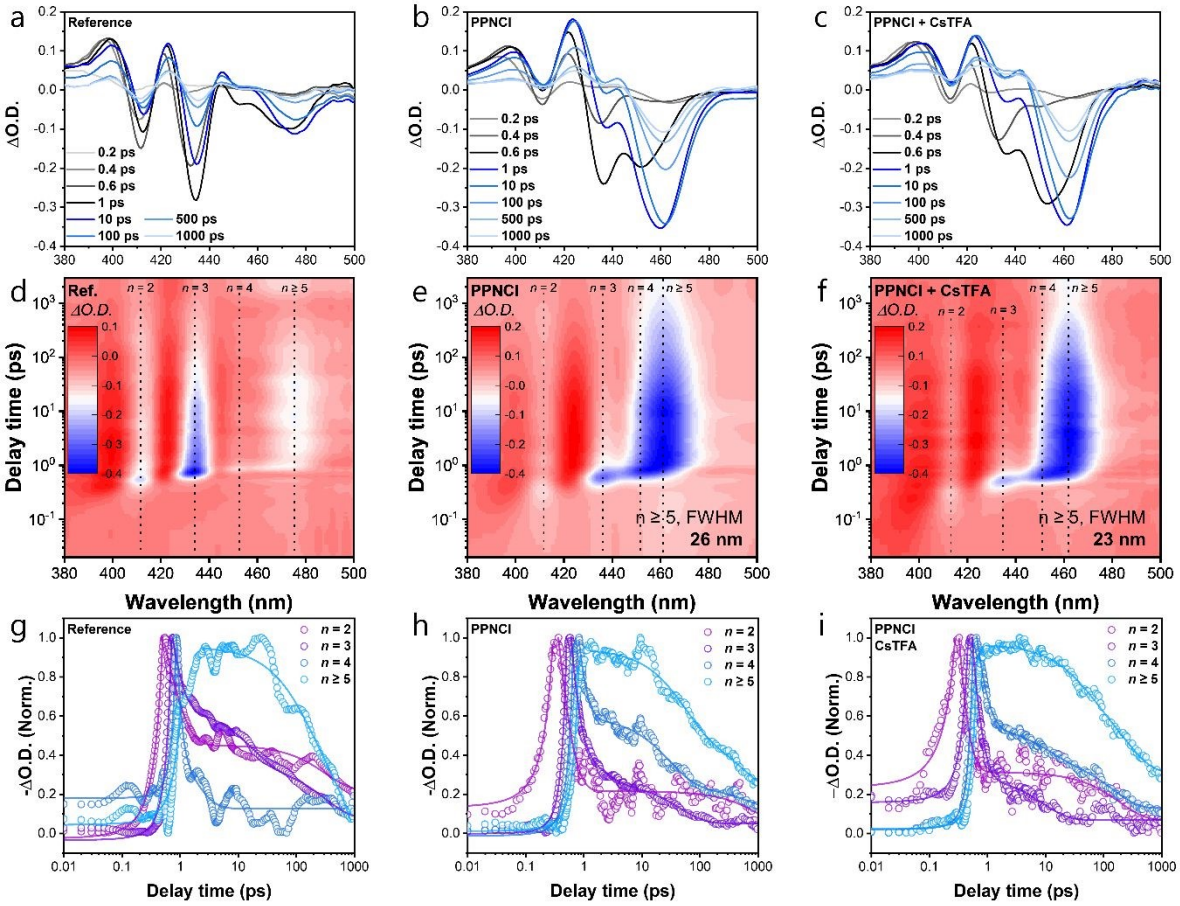

Figure 3. Phase distribution and carrier dynamics. TA spectra at selected timescales for (a) the reference, (b) PPNCl, and (c) PPNCl + CsTFA conditions. TA maps for (d) the reference, (e) PPNCl, and (f) PPNCl + CsTFA conditions. TA kinetics at n = 2, 3, 4, and ≥ 5 for (g) the reference, (h) PPNCl, and (i) PPNCl + CsTFA conditions.

consistent with the pronounced narrowing of the $n \geq 5$ GSB FWHM observed by TAS, suggesting effective defect passivation in the radiative phase. In agreement with the TAS analysis, the average PL lifetime (τ_{Rad}) also decreased from 12.2 to 7.7 ns. Decoupling the PL decay parameters indicates a rapid acceleration of the radiative recombination process (**Figure S2, Table S3**). Notably, the radiative lifetime decreased from 72 to 24 ns, corresponding to a threefold increase in the radiative recombination rate (K_r). Because the overall PL lifetime and PLQY are governed by the competition between K_r and the non-radiative rate (K_{nr}), this substantial increase in K_r simultaneously shortens the overall τ_{avg} and drives the PLQY enhancement. This implies an accelerated radiative rate, which is also tied to the enhanced energy funneling; the rapid funneling increases the local exciton concentration in large-*n* phases, allowing the radiative process to effectively outcompete non-radiative pathways. Collectively, these results indicate that PPNCl and CsTFA mitigate *n*-phase imbalance, promote more efficient inter-phase energy transfer, and effectively passivate defects.

Principles of phase reconstruction

To elucidate how PPNCl and CsTFA alleviate quasi-2D *n* phase imbalances, NMR measurements were performed using mixtures of PEABr (spacer) and the additives with systematically varied composition ratios. Notably, PPNCl has been reported to exhibit three distinct resonance signatures, consistent with multiple resonance-stabilized structures **(Figure S3a).**[4] In the PPN framework, the highly electronegative nitrogen atoms in the symmetric P–N bonds polarize electron density, imparting elevated electron density and partial negative character to the nitrogen sites. This electronic feature enables the $[PPN]^+$ cation to behave as a cationic electron donor and to engage in hydrogen bonding with the ammonium moiety of PEA^+.[4] As shown in **Figure 4a and Figure S3b**, ^{1}H NMR spectra of PEABr displayed concentration-dependent chemical-shift changes exclusively for protons associated with the ammonium group upon addition of PPNCl, supporting hydrogen-bond formation between the PEA^+ ammonium and $[PPN]^+$. The progressive downfield shift of the ^{1}H signal (peak f) reflects de-shielding and suggests the formation of weak hydrogen bonds between the ammonium protons of PEA^+ and the nitrogen lone pair of $[PPN]^+$. A comparable shift trend was also observed for PEABr in the presence of CsTFA (**Figure 4b**), suggesting that the highly electronegative fluorine atoms in TFA^- likewise form hydrogen bonds with the ammonium group of PEA^+.[25] Collectively, these results indicate that hydrogen-bond-mediated interactions between PEA^+ and the additives contribute to the redistribution and stabilization of quasi-2D *n* phases within the perovskite film. In addition, ^{31}P NMR (PPNCl) and ^{19}F NMR (CsTFA) revealed interactions not only with PEA^+ but also with Pb^{2+}. Specifically, both PPNCl and CsTFA were found to coordinate with Pb^{2+}, accompanied by electron withdrawal from Pb^{2+} toward the highly electronegative atoms of the additives, which manifests as lower chemical shifts in the ^{31}P and ^{19}F spectra (**Figure S4a, b**). These observations are consistent with XPS, where the Pb 4*f* binding energy increased upon interaction with PPNCl and CsTFA, indicating reduced electron density around Pb. Furthermore, the diminished metallic Pb signal provides additional evidence that these additives effectively passivate halide-vacancy-related defects (**Figure 4c**). In summary, PPNCl and CsTFA act as Lewis-base species that passivate Pb^{2+} through direct interactions, while simultaneously forming hydrogen bonds with the spacer cation. This hydrogen bonding restricts spacer mobility and retards their insertion into the perovskite framework, kinetically suppressing the formation of detrimental low-*n* phases.[16] Consequently, these cooperative interactions promote redistribution of the phase composition and enhance quasi-2D phase stability, as schematically illustrated in **Figure S5**.

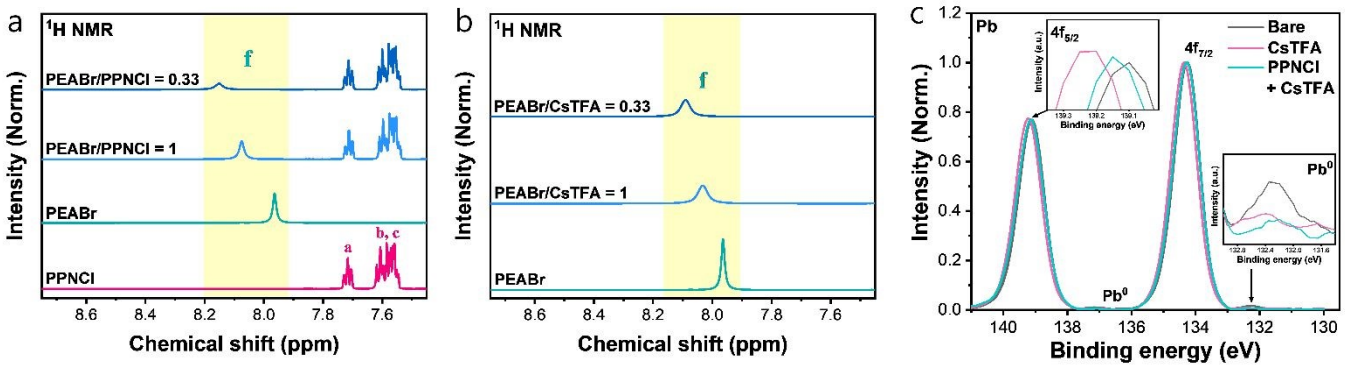

Figure 4. Interaction between spacers and additives. (a) ^{1}H NMR spectrum of PEABr and PPNCl. (b) ^{1}H NMR spectrum of PEABr and CsTFA. (c) Pb 4*f* binding energy spectra of quasi-2D films with and without additives

Optimized device results

To overcome limited hole injection, typically more challenging than electron injection in blue-emitting perovskite LEDs, TCTA was introduced as an interfacial hole-transporting layer (HTL) to optimize the device architecture (**Figure 5a**). When inserted between PEDOT:PSS and the perovskite, TCTA provides well-aligned energy levels (HOMO: −5.8 eV; LUMO: −2.4 eV) that promote hole transport (h^+) while effectively blocking electron leakage (e^-), thereby improving carrier-injection balance and enabling an optimized device configuration (**Figure 5b**). Beyond energetics, TCTA, owing to its carbazole-based structure, can exhibit superior wettability toward the DMSO-based perovskite precursor solution compared with polymeric HTLs such as poly-TPD and PVK,[26,27] leading to

improved quasi-2D film coverage. This morphological advantage is evidenced by a pronounced reduction in surface roughness, with the RMS roughness decreasing from 16 nm on PEDOT:PSS (without TCTA) to 7.65 nm on TCTA (**Figure S6**). Consistent with these combined advantages, incorporation of TCTA substantially reduces leakage current and enhances both efficiency and luminance. Consequently, the optimized device delivers pure-blue electroluminescence at 473 nm with a maximum EQE of 8% and a peak luminance of 350 cd/m^2 (**Figure 5c, d**). Importantly, this optimized quasi-2D LED demonstrates exceptional color stability under continuous electrical operation. As illustrated in **Figure 5e**, the normalized EL spectra maintain a consistent emission profile with a negligible peak shift (ΔPeak of 3 nm) across a range of applied driving voltages from 3.3 V to 5.7 V. Device-to-device statistics for the optimized condition are summarized in **Figure S7**. Although devices fabricated under the same conditions exhibited batch-to-batch variation in the emission peak position (471–474 nm), the EL peak shift during operation remained within 3 nm,

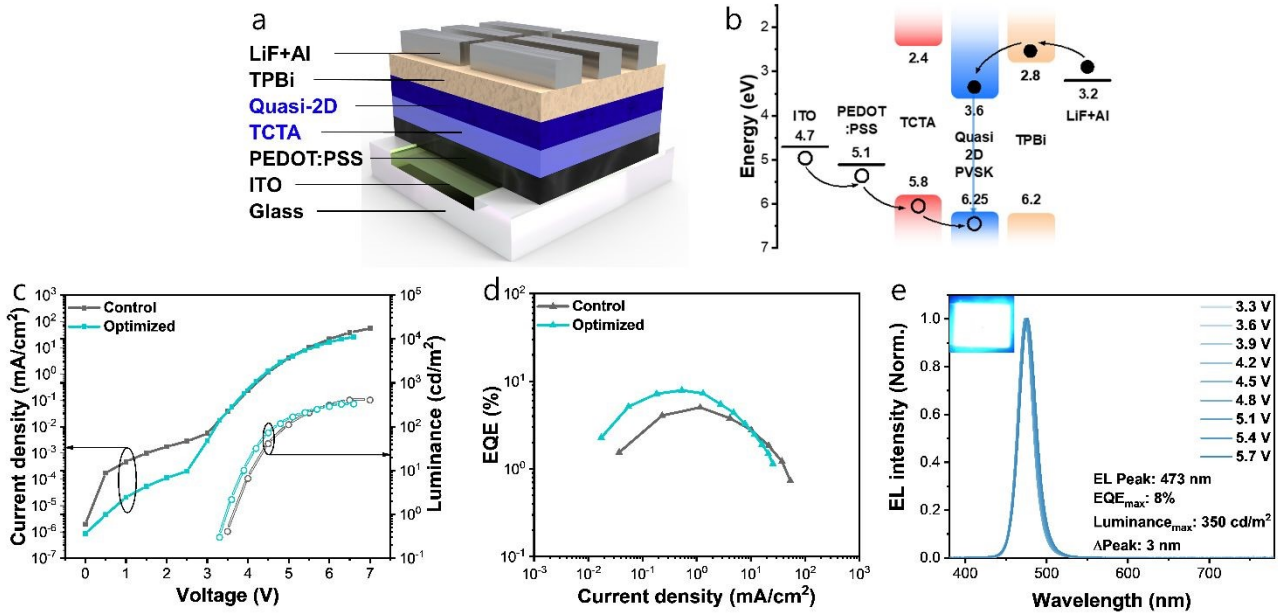

Figure 5. Characterization of the optimized perovskite LED. (a) schematic of device structure, (b) band diagram of optimized quasi-2D perovskite LED structure. (c) Current density-voltage-luminance (J-V-L) curves. (d) Current density-external quantum efficiency (J-EQE) curves. (e) EL Spectra of optimized quasi-2D LED. The inset shows a photograph of the operating device.

demonstrating excellent spectral stability. To highlight the superiority of our approach, we compared the performance of our device with previously reported pure-blue mixed-halide perovskite LEDs (**Figure S8, Table S4**). As summarized in Figure S8, our device demonstrates one of the best performances to date when simultaneously considering the minimized peak shift and narrow FWHM.

Conclusions

Efficient pure-blue emission from quasi-2D perovskites demands tight control over the *n*-phase distribution, while mitigating phase segregation in mixed-halide systems requires effective defect passivation. Here, PPNCl and CsTFA were introduced as multifunctional additives that simultaneously modulate spacer-perovskite binding and passivate Pb^{2+}-related defects. In PPNCl, Cl^- widens the bandgap of quasi-2D domains to enable pure-blue emission, whereas $[PPN]^+$ acts as an electron-donating cation and forms hydrogen bonds with the ammonium group of PEA^+, thereby strengthening spacer-perovskite interactions and promoting reconstruction of the quasi-2D *n* phase landscape. Likewise, TFA^- drives *n*-phase redistribution, plausibly through the strong electronegativity of its F substituents and hydrogen-bonding interactions with PEA^+. As a consequence, the population of low-*n* phase ($n = 2$), major channels for non-radiative recombination, was substantially reduced, and inter-phase energy transfer was enhanced, as supported by TAS analysis. In parallel, the additives passivated halide vacancies and suppressed metallic Pb formation, further lowering non-radiative losses. Compared with devices optimized solely by adjusting the $PbBr_2/PbCl_2$ ratio, this additive-enabled strategy delivered markedly improved spectral stability. The resulting LEDs exhibited pure-blue electroluminescence at 473 nm with a maximum EQE of 8%, a maximum luminance of 350 cd/m^2, and a narrow FWHM of 21 nm. During operation, the EL peak shift was constrained to within 3 nm, demonstrating robust color stability. Overall, these results provide an effective route to stabilizing mixed-halide quasi-2D perovskite emitters and advance the development of efficient, spectrally stable pure-blue perovskite LEDs.

Data availability

The data supporting the findings of this study are available within the article and its supplementary information.

View Article Online
DOI: 10.1039/D6FD00036C

Author contributions

Jinu Park and Seoyeon Park contributed equally to this work.
Jinu Park: Conceptualization, Data Curation, Formal Analysis, Investigation, Methodology, Validation, Visualization, Writing – original draft, Writing – review & editing.
Seoyeon Park: Data Curation, Formal Analysis, Validation, Writing – original draft, Writing – review & editing.
Seongju Park: Data Curation, Formal Analysis, Investigation.
Hyunjin Cho: Formal Analysis, Investigation, Methodology.
Doh C. Lee: Methodology, Resources.
Byungha Shin: Funding acquisition, Project administration, Resources, Supervision, Writing – review & editing.

Conflicts of interest

There are no conflicts to declare.

Acknowledgements

This work was supported by the National Research Foundation of Korea(NRF) grant funded by the Korea government(MSIT) (No. RS-2022-NR068162).

Notes and references

1. Han, T. H. *et al.* A roadmap for the commercialization of perovskite light emitters. *Nat. Rev. Mater.* **7**, 757–777 (2022).
2. Gao, Y. *et al.* Microsecond-response perovskite light-emitting diodes for active-matrix displays. *Nat. Electron.* **7**, 487–496 (2024).
3. Pacchioni, G. Highly efficient perovskite LEDs. *Nat. Rev. Mater.* **6**, 108 (2021).
4. Yuan, S. *et al.* Efficient blue electroluminescence from reduced-dimensional perovskites. *Nat. Photonics* **18**, 425–431 (2024).
5. Ma, C. *et al.* Recent progress in perovskite light-emitting diodes with high external quantum efficiency and stability. *CrystEngComm* **27**, 3853–3876 (2025).
6. Bai, W. *et al.* Perovskite Light-Emitting Diodes with an External Quantum Efficiency Exceeding 30%. *Adv. Mater.* **35**, 1–8 (2023).
7. Baek, S. D. *et al.* Grain engineering for efficient near-infrared perovskite light-emitting diodes. *Nat. Commun.* **15**, 1–10 (2024).
8. Jiang, J. *et al.* Red Perovskite Light-Emitting Diodes with Efficiency Exceeding 25% Realized by Co-Spacer Cations. *Adv. Mater.* **34**, 2–9 (2022).
9. Gao, Y. *et al.* Highly efficient blue light-emitting diodes based on mixed-halide perovskites with reduced chlorine defects. *Sci. Adv.* **10**, (2024).
10. Lee, S. *et al.* Brightening deep-blue perovskite light-emitting diodes: A path to Rec. 2020. *Sci. Adv.* **10**, (2024).
11. Seo, S. J., Park, S. & Jang, H. W. Flexible Micro-LEDs: Advanced Fabrication Techniques and Applications. *Electron. Mater. Lett.* **21**, 311–330 (2025).
12. Kumawat, N. K. *et al.* Band Gap Tuning of CH3NH3Pb(Br1-xClx)3 Hybrid Perovskite for Blue Electroluminescence. *ACS Appl. Mater. Interfaces* **7**, 13119–13124 (2015).
13. Chen, Y. *et al.* All-site alloyed perovskite for efficient and bright blue light-emitting diodes. *Nat. Commun.* **16**, 1–6 (2025).
14. Liu, Y. *et al.* Efficient blue light-emitting diodes based on quantum-confined bromide perovskite nanostructures. *Nat. Photonics* **13**, 760–764 (2019).
15. Park, J. *et al.* Efficient and spectrally stable pure blue light-emitting diodes enabled by phosphonate passivated CsPbBr3 nanoplatelets with conjugated polyelectrolyte-based energy transfer layer. *EcoMat* **6**, 1–13 (2024).
16. Park, S. *et al.* Controlling the Phase Distribution of Single Bromide Quasi-2-Dimensional Perovskite Crystals via Solvent Engineering for Pure-Blue Light-Emitting Diodes. *ACS Appl. Mater. Interfaces* **16**, 38395–38403 (2024).
17. Hangleiter, A. & Hacker, R. PHYSICAL REVIEW LETTERS 9 JUr V1990 Enhancement of Band-to-Band Auger Recombination by Electron-Hole Correlations. **65**, 215–218 (1990).
18. Wang, F., Wu, Y., Hybertsen, M. S. & Heinz, T. F. Auger recombination of excitons in one-dimensional systems. *Phys. Rev. B - Condens. Matter Mater. Phys.* **73**, 1–5 (2006).
19. Jiang, Y. *et al.* Reducing the impact of Auger recombination in quasi-2D perovskite light-emitting diodes. *Nat. Commun.* **12**, 336 (2021).

20. Xing, J. *et al.* Color-stable highly luminescent sky-blue perovskite light-emitting diodes. *Nat. Commun.* **9**, 1–8 (2018).
21. Yuan, M. *et al.* Perovskite energy funnels for efficient light-emitting diodes. *Nat. Nanotechnol.* **11**, 872–877 (2016).
22. Zhu, H. *et al.* High-performance hysteresis-free perovskite transistors through anion engineering. *Nat. Commun.* **13**, 1–8 (2022).
23. Karlsson, M. *et al.* Role of chloride on the instability of blue emitting mixed-halide perovskites. *Front. Optoelectron.* **16**, 1–10 (2023).
24. Kim, M., Lee, H., Kim, K. & Kim, J. Structural Continuity and Orientation Effects of Organometallic Perovskites. *Electron. Mater. Lett.* **21**, 790–799 (2025).
25. Kuang, Y. *et al.* High-Performance Pure Red Quasi-Two-Dimensional Perovskite Light-Emitting Diodes with Bifunctional Potassium Trifluoroacetate Additive. *ACS Mater. Lett.* **5**, 2922–2928 (2023).
26. Tseng, Y. T., Chen, T. Y. & Chu, S. Y. A simple hole transport composite single-layer for high-efficiency quantum dot light-emitting diodes and exploring its feasibility for flexible applications. *J. Alloys Compd.* **1049**, 185378 (2025).
27. Teng, Y. H. *et al.* Enhancing Sky-Blue Perovskite Light-Emitting Diode Performance through Guanidinium-Based Dual-Functional Molecular Engineering. *ACS Appl. Mater. Interfaces* **18**, 7189–7201 (2026).

View Article Online
DOI: 10.1039/D6FD00036C

Phase Regulation via Dual Additives for Pure-blue Emitting Quasi-2D Perovskite Light Emitting Diodes

Jinu Park,*[a] Seoyeon Park,*[a] Seongju Park,[a] Hyunjin Cho,[b] Doh C. Lee[b] and Byungha Shin†[a]

a) Department of Materials Science and Engineering, Korea Advanced Institute of Science and Technology (KAIST), Daejeon 34141, Republic of Korea

b) Department of Chemical and Biomolecular Engineering, Korea Advanced Institute of Science and Technology (KAIST), Dae-jeon 34141, Republic of Korea

†Corresponding authors: byungha@kaist.ac.kr

Data availability

The data supporting the findings of this study are available within the article and its supplementary information.